

Addendum V to ATBD

T. Meissner, F. Wentz and D. Le Vine

with contributions from S. Brown, E. Dinnat, L. Hong, J. Gales, A. Manaster, P. de Matthaeis, S. Misra, A. Santos-Garcia, Y. Soldo

November 13, 2017

This addendum documents the changes made to the ATBD between release of V4.0 and V5.0 of the Aquarius L2 salinity retrieval algorithm and included in V5.0. Prior to release of V5.0 the code was updated to include all the changes described here and then the entire data set was rerun.

In brief, the changes to the salinity retrieval algorithm from V4.0 to V5.0 are:

1. The source of the ancillary sea surface temperature (SST) field has been changed from the NOAA OI SST to the SST field from the Canadian Meteorological Center (CMC).
2. The reference sea surface salinity (SSS) field that is used in the sensor calibration and in the derivation of TA_expected (i.e. forward algorithm) has been changed from HYCOM SSS to the analyzed monthly Scripps ARGO SSS.
3. The model for the component of celestial radiation reflected from the surface into the radiometer antenna has been updated based on a model derived from the difference between fore and aft observations of the SMAP (Soil Moisture Active Passive Mission) L-band radiometer. The advantage of this approach is that it includes both the effects of the model for celestial radiation at L-band and the effect of surface roughness.

4. The empirical symmetrization correction which corrects asc/dsc differences has been rederived to reflect improvements in the correction for the reflected galaxy.
5. The model for absorption by atmospheric oxygen has been changed from Wentz and Meissner (2016) to Liebe et al. (1992).
6. Various components of the surface roughness correction model have been updated from the model of Meissner et al. (2014):
 - a. The SST dependence of the wind induced emission has been adjusted.
 - b. The correction table depending on wind speed and VV radar backscatter has been updated.
 - c. The correction table depending on wind speed and significant wave height (SWH) has been omitted.
 - d. The 1st guess SSS field that is used in the HHH wind speed retrieval (Addendum III, section 2) has been updated.
7. A few changes have been made to the sensor calibration and calibration drift correction:
 - a. When calculating the global average of $TA_{\text{measured}} - TA_{\text{expected}}$ in the sensor calibration, the observations are filtered for rain using the instantaneous rain rate from the Aquarius RA product (see item 9).
 - b. A small channel dependent constant offset is added to the measured specular surface brightness temperature $TB_{\text{sur},0}$ in order to ensure matching between measured and expected TB and between measured and reference SSS and thus enforcing closure between sensor calibration and salinity retrievals.
8. In the maximum likelihood estimate (MLE) of the salinity retrieval algorithm, V-pol and H-pol have equal weight.

9. The L2 files include instantaneous rain rates based on the NOAA CMORPH rain product. They are used to filter data for rain in the calibration drift correction and also for validating the Aquarius salinity versus ARGO in-situ measurements.

1 Ancillary Sea Surface Temperature Field

Up to and including V4.0 the ancillary SST field was the NOAA Optimum Interpolated (OI) SST. An evaluation of the performance of the SSS retrieval algorithm has been performed comparing various ancillary SST fields (Meissner et al., 2016). The result of the analysis was that the best performance is obtained with the daily GHRSSST (Gridded High-Resolution SST) Level 4 field from the Canadian Meteorological Center (CMC). It is gridded at 0.2° resolution and available from the PO.DAAC web site (<https://podaac.jpl.nasa.gov/dataset/CMC0.2deg-CMC-L4GLOB-v2.0>). Version 5.0 uses this ancillary SST field.

2 Reference Salinity Field

The reference salinity field, SSS_{ref} , is used in the sensor calibration and calibration drift correction. The unknown constants in the radiometer calibration (effectively, gain and offset) are adjusted so that the global average SSS from Aquarius matches the global average of the reference SSS field. This is done in two steps, first removing an exponential fit to the radiometer drift and then using a 7-day running average to remove the remaining “wiggles”. For details see Addendum II section IV. The SSS_{ref} is also needed for deriving the GMF for the wind induced surface emission. The GMF derivation is done empirically by computing the difference between the measured Aquarius surface TB and the TB computed for a flat ocean surface using the reference salinity field. For details see Meissner et al. (2015) and Addendum III, Section 4. The SSS_{ref} enters in the computation of TB for a flat ocean surface.

Up to and including V4.0 We used the salinity field from HYCOM (www.hycom.org) as SSS_{ref} . When compared with actual in-situ measurements from ARGO floats, it was found that the HYCOM field has spurious salty biases in the tropics (Figure 1) and also that a model change in early 2013 results in small jump in the mean global salinity (Figure 2). For V5.0 the

monthly 1-degree gridded interpolated ARGO SSS field provided by Scripps (http://www.argo.ucsd.edu/Gridded_fields.html) will be used for the reference salinity.

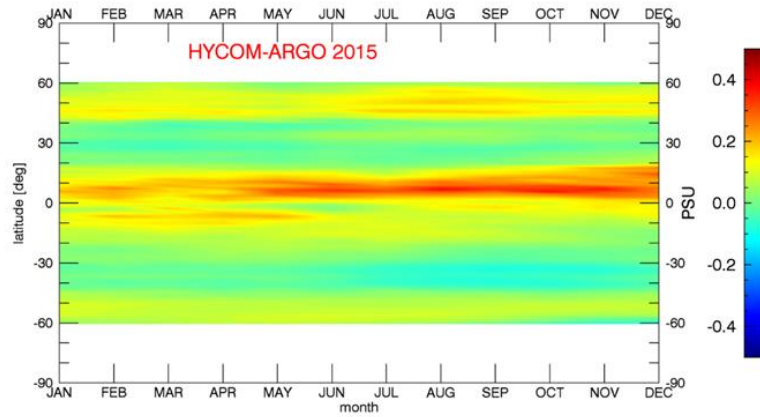


Figure 1: Hovmoeller diagram of HYCOM – Scripps ARGO SSS for the year 2015.

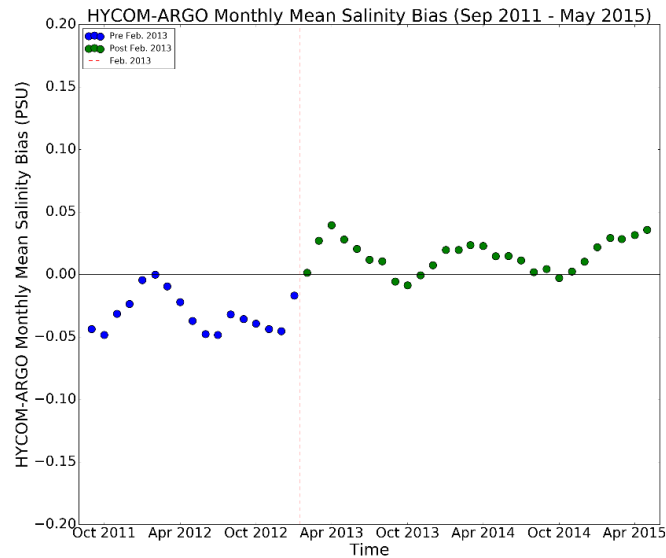


Figure 2: Time series of global monthly difference between HYCOM and Scripps ARGO SSS.

3 Reflected Galaxy

One major goal in the development of the Aquarius V5.0 salinity algorithm is an improvement of the correction for L-band radiation from the galaxy that is reflected from the surface to the radiometer. The V4.0 algorithm used as a source the map for the galactic radiation by LeVine and Abraham [Le Vine and Abraham, 2004; Dinnat et al, 2010] convolved with the Aquarius antenna pattern and used a geometric optics model (i.e. statistical collection of tilted facets) for the ocean surface to account for roughness. In this model, the RMS slope characterizes the rough surface and in turn the RMS slope is determined by the surface wind speed. For details see ATBD Version 2, section 2.2 and Appendix A. The GO model removes the reflected galactic radiation correctly to about 90%. The remaining 10% shows up as spurious signal in the Aquarius salinity retrieval and manifest itself in differences between the morning (descending) and the evening (ascending) swaths over the same ocean. In V3.0 an empirical correction was derived for this residual in the form of a zonal symmetrization of the TA from both swaths. For details see Addendum III. The main reason for the (10%) deficiency in the galactic reflection model is the uncertainty in (analytical) modeling of the rough surface. The aim for V5.0 was to improve the correction for galactic reflection and reduce magnitude of the empirical symmetrization correction.

3.1 Analysis of SMAP Fore - Aft Observations

Observations from the SMAP (Soil Moisture Active and Passive) mission, that has been making passive L-band observation since April 2015, provide a very good opportunity to improve the correction for the reflected galactic signal. SMAP performs a full 360° scan and thus observes each location almost simultaneously in forward (fore) and backward (aft) direction. The (relatively) strong reflected radiation emanating from the plane of the galaxy can appear in both the forward and the backward look but usually not at the same time. Radiation from directions other than the plane of the galaxy are generally quite small (Le Vine and Abraham,

2004). If all other signals that depend on look direction (Faraday rotation, wind direction, solar and lunar radiation) have been accurately removed, then taking the difference between fore and aft measured TA produces the galactic radiation:

$$T_{A,gal}(\phi_{fore}) - T_{A,gal}(\phi_{aft}) = T_A(\phi_{fore}) - T_A(\phi_{aft}) \quad (1)$$

This equation can be used to *derive an empirical galactic correction* separate for the SMAP fore and aft looks. For example, looking for cases where the signal from the aft look is small (< 2K) and assuming that the model (theory) for the SMAP aft look reflected galactic radiation is correct if it is smaller than 2 K, then the empirical correction for the fore look can then be obtained from (1) as:

$$T_{A,gal,emp}(\phi_{fore}) = T_{A,meas}(\phi_{fore}) - T_{A,meas}(\phi_{aft}) + T_{A,gal,model}(\phi_{aft}) \quad (2)$$

Likewise, assuming that the computed SMAP fore look galaxy model is correct if it is smaller than 2 K, then the empirical galaxy model for the aft look can then be obtained from (1) as:

$$T_{A,gal,emp}(\phi_{aft}) = T_{A,meas}(\phi_{aft}) - T_{A,meas}(\phi_{fore}) + T_{A,gal,model}(\phi_{for}) \quad (3)$$

When performing the analysis, observations were discarded for which the reflected solar radiation is not negligible. Reflected solar radiation differs between fore and aft looks and currently the correction for reflected solar radiation in the SMAP algorithm is not accurate enough. It is possible to find observations for all times and orbit positions for which both the reflected solar radiation is negligible and either the TA galaxy of the fore or the aft look are less than 2 K. Therefore, it is possible to derive empirical galactic corrections for SMAP sensor for both look directions using equations (2) and (3). Separate derivations are performed for different wind speed regimes, which consist of 5 m/s intervals.

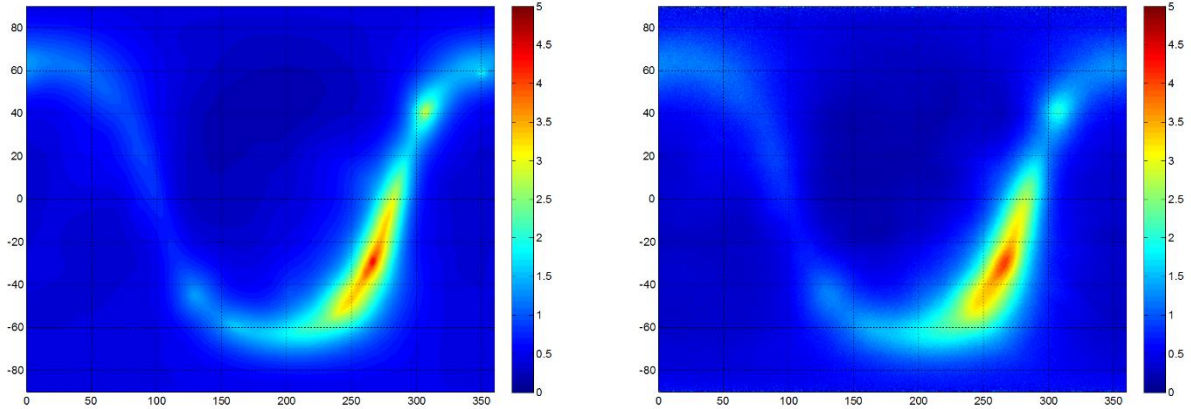


Figure 3: Left: GO model for the SMAP reflected galaxy based on ATBD, Version 2 (Section 2.2 and Appendix A). Right: Empirically derived SMAP reflected galaxy based on fore – aft analysis using equations (2) and (3) in this addendum. In obtaining these figures all observations were averaged together independent of wind speed.

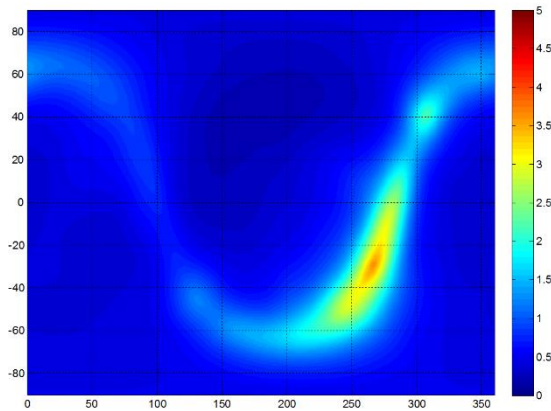


Figure 4: GO model for the SMAP reflected galaxy adding 2 m/s to the wind speed when calculating the slope variance.

The largest part of the SMAP fore – aft results can be reproduced using a tilted facet calculation as explained in the ATBD Version 2 section 2.2 and Appendix A, but adding 2 m/s to the wind speed w when calculating the RMS slope variance $\sigma^2(W)$ according to ATBD Version, Appendix A, equation (A11). The value of $\sigma^2(W)$ enters the tilted facet integration in the GO

model. The effective increase in wind speed means that the surface roughness at L-band frequencies in the GO model needs to be increased and this increase brings the slope variance from equation A11 in ATBD Version 2 closer to the Cox-Munk value (equation A10 in ATBD Version 2). This is shown in Figure 3, Figure 4 and Figure 5. In addition to this increase of the surface roughness, there are other modifications, which are explained in detail in the following section.

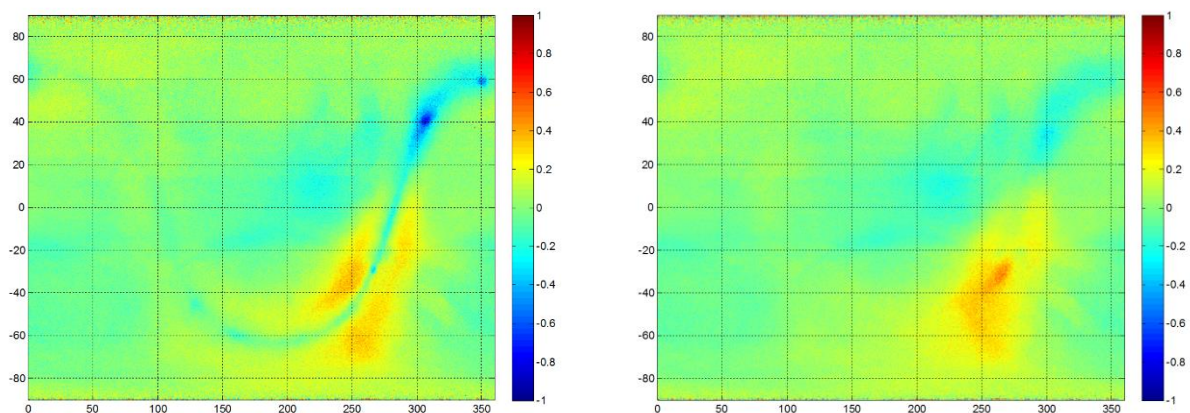


Figure 5: Left: Difference between the galactic map derived from SMAP fore – aft and the GO calculation (ATBD Version 2 section 2.2. + Appendix A). Right: Difference between the galactic map derived from SMAP fore – aft and the modified GO calculation adding 2 m/s in the calculation of the RMS slope. In obtaining these figures all observations were averaged together independent of wind speed.

3.2 Implementation of the SMAP Fore – Aft Results into the Aquarius Algorithm

The first step in computing the Aquarius V5 antenna temperature of the reflected galaxy ($T_{A,gal}$) is to compute the geometric optics value ($T_{A,go}$). $T_{A,go}$ is a function of time ($t =$ sidereal year), the intra-orbit position of the Aquarius spacecraft (ϕ), and sea-surface wind speed (W). Tables of $T_{A,go}(t, \phi, W)$ are pre-computed using the Aquarius on-orbit simulator. For operational processing, $T_{A,go}$ for a given observation is found from a tri-linear interpolation of the $T_{A,go}(t, \phi, W)$ table. There are nine separate tables corresponding to the 3 horns and the first 3 Stokes parameters. The Aquarius ATBD Version 2 (section 2.2 and Appendix A) gives the details of how this is done.

To implement the SMAP-derived adjustments, 2 m/s is added to the wind when computing $T_{A,go}$ as described in the paragraph above. The SMAP results (Section 3.2) indicated the smoothing of the galaxy radiation due to (1) the integration over the Aquarius antenna and (2) the scattering from the rough ocean surface was greater than predicted by the geometric optics model. Adding 2 m/s to the input wind speed mitigated this problem.

After adding the 2 m/s, there is still some residual differences between the SMAP derived galaxy and $T_{A,go}$. To remove the residuals, adjustment tables are computed. These tables are a function of the galactic longitude α , galactic latitude β , and wind speed W . The tables are denoted by $\Delta T_{A,go}(\alpha, \beta, W)$, and there are separate tables for v-pol and h-pol.

Let $T_{A,smap}$ be the reflected galactic T_A found directly from the fore-minus-aft SMAP differences. Let $T_{A,go}(t, \phi, W+2)$ be the reflected T_A from the geometric optics model with 2 m/s added to the wind. The adjustment table $\Delta T_{A,go}(\alpha, \beta, W)$ is then found by averaging over a year of SMAP observations.

$$\Delta T_{A,go}(\alpha, \beta, W) = \left\langle T_{A,smap} - T_{A,go}(t, \phi, W + 2) \right\rangle_{\alpha, \beta, W} \quad (4)$$

where the brackets indicated a one-year average into 0.25° α -bins, 0.25° β -bins, and 5 m/s wind bins. The reflected galactic T_A used for Aquarius processing is then

$$T_{A,gal} = T_{A,go}(t, \phi, W + 2) + \Delta T_{A,go}(\alpha, \beta, W) \quad (5)$$

An additional constraint is applied to this procedure. Results indicated that the polarization ratio (v-pol/h-pol) for $T_{A,smap}$ was somewhat noisy. Accordingly, we constrain the polarization ratio of the SMAP-derived reflected galaxy to be the polarization ratio predicted by geometrics optics. The following scaling accomplishes this:

$$T_{A,smap,v} = T_{A,smap,h} \frac{T_{A,go,v}(t, \phi, W + 2)}{T_{A,go,h}(t, \phi, W + 2)} \quad (6)$$

Thus, we rely just on the h-pol $T_{A,smap}$ to characterize galactic reflections. The surface reflectivity of h-pol is about twice that of v-pol, and hence h-pol has the stronger galactic signal (i.e. greater signal-to-noise).

The changes in the Aquarius reflected galaxy based on the SMAP fore – aft look results are shown in Figure 6 for horn 2 as an example.

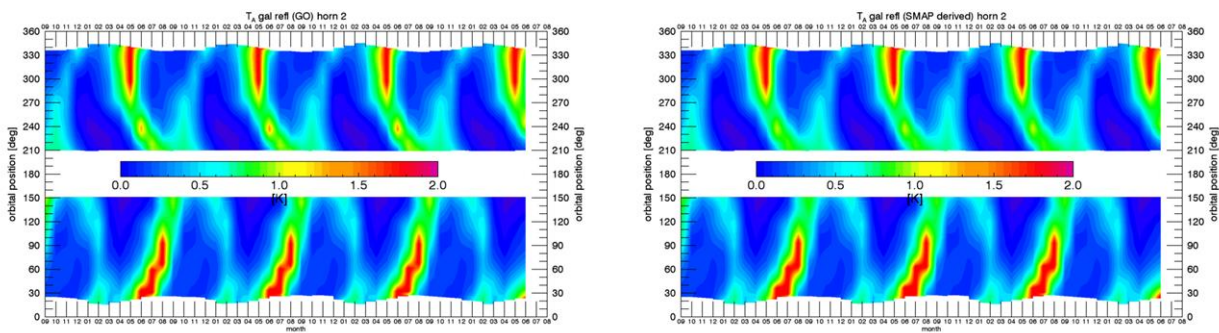


Figure 6: Reflected galaxy for Aquarius horn 2. Left: GO calculation as specified in ATBD, Version 2. Right: GO calculation after the adjustments based on the SMAP fore – aft look.

These changes are applied in the calculation of the reflected galaxy radiation. The calculation of the direct galaxy radiation has not been changed from ATBD Version 2 and is still using the original galactic maps of Le Vine and Abraham (2004) and Dinnat et al. (2010).

In order to evaluate the improvement of the SMAP derived adjustments to the reflected galaxy, the Aquarius salinity retrievals were run first with the GO galaxy using the parameters from the ATBD Version 2 and then with the SMAP derived adjustments. The improvements in TA measured minus expected are shown in Figure 7.

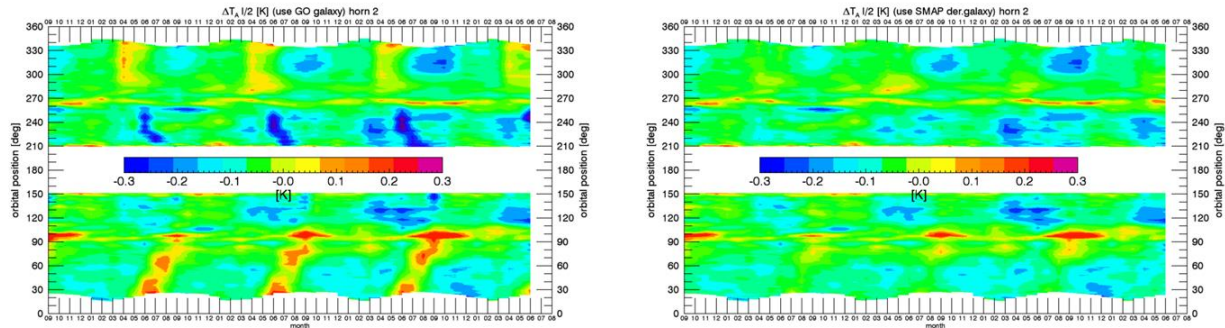


Figure 7: Measured minus expected TA for Aquarius horn 2. Left: GO calculation as specified in ATBD, Version 2. Right: GO calculation after the adjustments based on the SMAP fore – aft look. For the calculation of TA expected in this figure we have used HYCOM as reference SSS.

3.3 Empirical Symmetrization

Another important metric for the assessment of the accuracy of the galactic correction are the differences between ascending and descending swaths. The results are shown in Figure 8.

The new model clearly reduces the difference between ascending – descending passes over the same ocean. However, some residual ascending – descending biases still remain even with the improved galaxy model. The remaining differences are removed empirically using the zonal symmetrization correction, Δ , introduced for the Aquarius V3.0 and V4.0 releases. For details see Addendum III, section 5.4. For the V5.0 release the derivation of the zonal symmetrization correction has been repeated following the same method as explained in Addendum III section 5.4. but using the updated improved galactic correction (section 3.2 of this Addendum). The results are shown in Figure 9. The empirical symmetrization correction necessary to remove the residual ascending – descending biases is about half as large for V5.0 with the improved galactic reflection model than it was for V3.0 and V4.0.

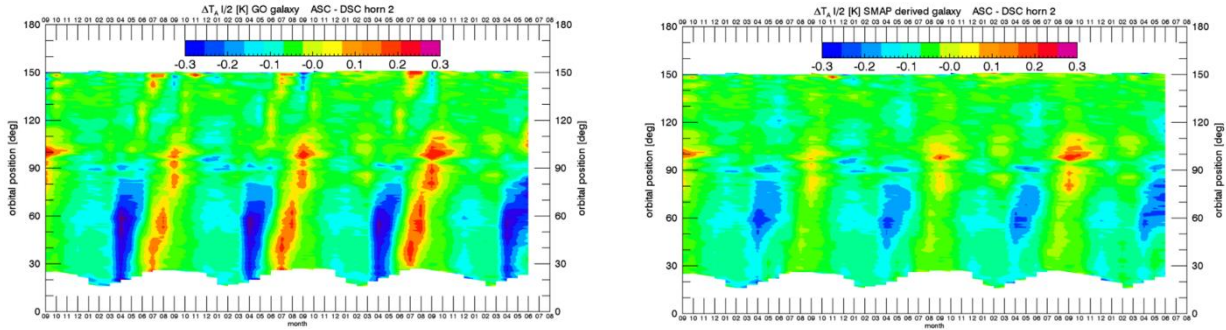


Figure 8: Left: Ascending – descending TA measured – expected for Aquarius horn 2 using reflected galaxy from the GO model in ATBD Version 2 section 2.2. + Appendix A. Right: Ascending – descending TA measured – expected for Aquarius horn 2 using reflected galaxy from the updated reflected galaxy model based on the SMAP fore – aft results (section 3.2 of this Addendum).

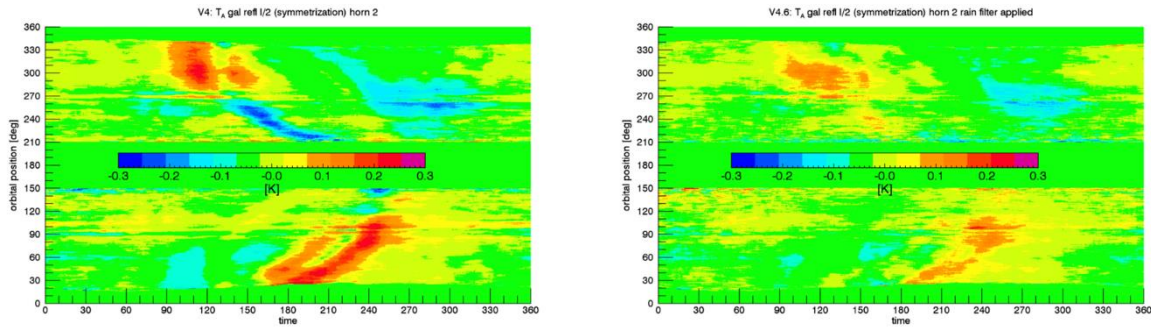


Figure 9: Empirically derived symmetrization correction $\Delta(z)$. Left: Based on the GO model (ATBD Version 2). This correction is used in the V3.0 and V4.0 releases. Right: Based on the improved galactic model (section 3.2 of this Addendum).

The Aquarius V5 Level 2 files contain both the values of the reflected galaxy TA from the GO calculation as given in ATBD version 2 and the final values that are used in the V5.0 algorithms after all the effective and empirical adjustments that were explained in this section (SMAP fore – aft results and the empirical symmetrization).

4 Oxygen Absorption Model

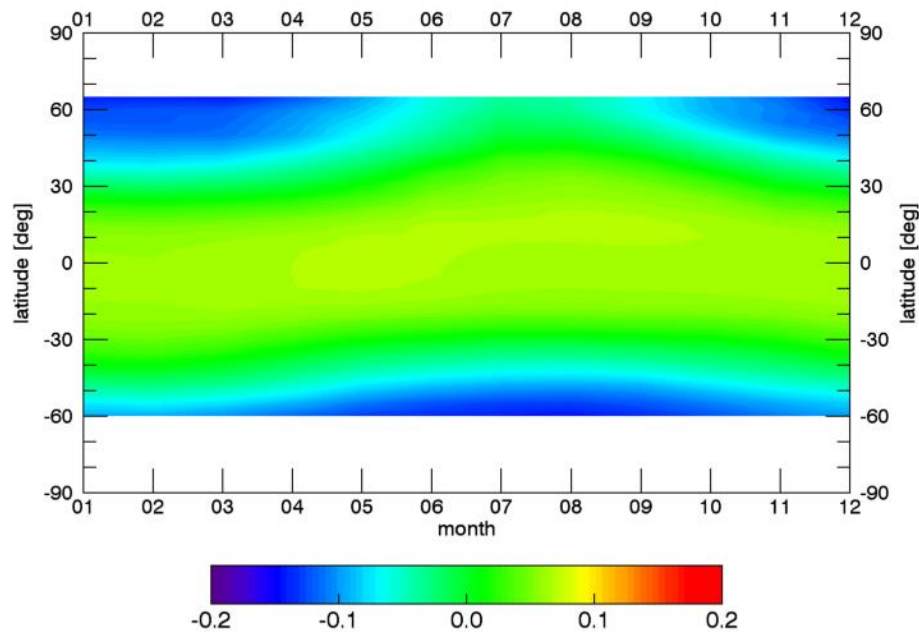


Figure 10: Effect of atmospheric absorption: Top of the atmosphere (TOA) minus surface (SUR) TB for h-pol horn 2. The figure shows the difference between the Liebe et al. (1992) O_2 absorption model, which is used in V5.0 and the Wentz Meissner (2016) O_2 absorption model, which is used in V4.0. In calculating this Hovmoeller diagram we have used all available Aquarius data.

The Aquarius V4.0 salinity retrievals show spurious seasonal salty biases at high N and S latitudes, which are largest the N Pacific during April and May. These biases have been tracked back to the absorption model for atmospheric O_2 that is used in the atmospheric correction (ATBD version 2, section 3.5). Up to V4.0, the O_2 absorption model of Wentz and Meissner (2016) has been used for the atmospheric correction. The atmospheric absorption coefficient

$\gamma_{O, nr}$ (in dB/km) for the non-resonant O₂ absorption in the Wentz-Meissner (2016) model is given by:

$$\gamma_{O, nr} = 0.0056 \cdot (p + 1.1e) \cdot \theta^{1.5} \quad (7)$$

Here, $\theta = 300K / T_{air}$, T_{air} is the air temperature (in Kelvin), p is the dry air pressure (in hPa), and e is the water vapor pressure (in hPa). In the atmospheric correction, the variables T , p and e are taken from the ancillary NCEP atmospheric profiles for temperature, pressure and moisture.

For V5.0 the O₂ absorption model of Liebe et al. (1992) is used for the atmospheric correction. This helps to reduce the observed biases. The atmospheric absorption coefficient $\gamma_{O, nr}$ for the non-resonant O₂ absorption of this model is given by:

$$\gamma_{O, nr} = N \cdot 0.0056 \cdot (p + 1.1e) \cdot \theta^{0.8} \quad (8)$$

This change means that the dependence of the absorption coefficient on air temperature T_{air} has effectively been reduced in V5.0 by about 50% compared to V4.0. The normalization $N = 1.097687$ in (8) has been introduced so that for an average air temperature the global average atmospheric absorption correction $T_{B, TOA} - T_{B, SUR}$ stays the same in V5.0 as it had been in V4.0. The impact of changing the atmospheric absorption from (7) to (8) on the size of the atmospheric absorption correction $T_{B, TOA} - T_{B, SUR}$ is shown in Figure 10.

5 Surface Roughness Correction

The surface roughness correction (Addendum III, section 3) has been rederived for V5.0 using data corrected with the updated O₂ absorption model (Section 4), the updated model for the reflected galaxy (Section 3), the updated ancillary SST (Section 1) and the updated reference salinity field (Section 2). The roughness correction in V4.0 is given by three terms (eqn. 4 in Addendum III):

$$\Delta E_{rough} = \Delta E_{W0}(W_{HHH}, \varphi_r, T_S) + \Delta E_{W1}(W_{HHH}, \sigma'_{0,VV}) + \Delta E_{W2}(W_{HHH}, SWH) \quad (9)$$

The following changes have been made:

1. The SST dependence in the first term on the right, ΔE_{W0} has been modified (Section 5.1).
2. The correction table defining the second term, ΔE_{W1} , has been updated.
3. The third term, ΔE_{W2} , dependence on significant wave height (SWH) has been omitted.
4. The 1st guess SSS field used in the HHH wind speed retrieval (Addendum III, section 2) has been updated.

5.1 SST Dependence

The roughness correction is temperature dependent. This dependence is captured in the first term in equation (9) which now (Version 5.0) has the form:

$$\Delta E_{W0,p} = \delta_p(W, \varphi_r) \cdot \left[\frac{E_{0,p}(T_S)}{E_{0,p}(T_{ref})} + \rho'_p(T_S) \right] \quad p = V, H \quad (10)$$

where the change from V4.0 is the addition of the term ρ' . All of the other terms are unchanged. In particular, wind speed and directional dependence of $\delta_p(W, \varphi_r)$ is given as before by:

$$\delta_p(W, \varphi_r) = A_{0,p}(W) + A_{1,p}(W) \cdot \cos(\varphi_r) + A_{2,p}(W) \cdot \cos(2 \cdot \varphi_r) \quad (11)$$

The harmonic coefficients $A_{i,p}$ are given in Addendum III (eqn. 7) and have not been changed. They can also be found in Meissner et al. (2014) and have been used for V3.0 and V4.0. The expressions $E_{0,p}(T_s)$ are the emissivities of the ideal half-space (air above flat ocean surface) and given by the Fresnel reflectivity as before. The reference temperature, $T_{ref} = 20^\circ C$ as before.

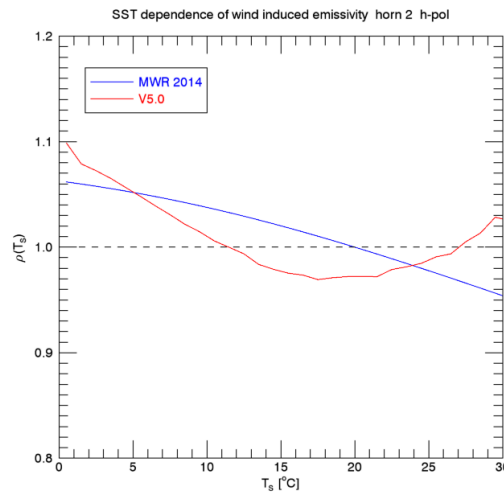


Figure 11: SST dependence of the wind induced emissivity for horn 2 h-pol. Black dashed line = no SST dependence. The blue line in the SST dependence from Meissner et al. (2014), which was used in V3.0. The red curve is the SST dependence $\rho(T_s)$ in equation (12) that is used in V5.0.

The additional term ρ'_p in eqn. (10) can be regarded as an empirically derived correction to the SST dependence of the GO model. In V5.0 this correction term has been added to the wind induced emissivity. That means that SST dependence of the wind-induced emissivity ΔE_{w0} in V5.0 is effectively given by:

$$\rho_p(T_S) = \frac{E_{0,p}(T_S)}{E_{0,p}(T_{ref})} + \rho'_p(T_S) \quad (12)$$

The form of $\rho(T_S)$ for horn 2 h-pol is shown in Figure 11. The values for $\rho'(T_S)$ are tabulated in Table 2 of Appendix A of this Addendum as function of T_S for the 6 Aquarius channels.

Making this modification to the wind induced emissivity model is supported by the data for low and intermediate wind speeds $W < W_c = 11 \text{ m/s}$. At high wind speeds $W \geq W_c = 11 \text{ m/s}$ the value of the additional term in (10) is kept constant at its value at W_c , which is also supported by the data. That means that for high wind speeds $W \geq W_c$ the term $\Delta E_{w0,p}$ from eqn. (9) is given by:

$$\Delta E_{w0,p} = \delta_p(W, \varphi_r) \cdot \frac{E_{0,p}(T_S)}{E_{0,p}(T_{ref})} + \delta_p(W_c, \varphi_r) \cdot \rho'_p(T_S) \quad (13)$$

and the slope of $\Delta E_{w0}(W_S)$ at high wind speeds is still the same for V5.0 as the one derived in Meissner et al. (2014) and used in V4.0. There are several physical mechanisms that can cause microwave emission from the wind roughened surface (tilted facets, Bragg scattering

from capillary waves, emission from sea foam or sea spray, ...). These mechanisms have different magnitudes in different wind speed regimes and it is possible that they also have different dependence on SST. That is to say, the SST dependence of ΔE_{w0} can be different at high winds than at low or intermediate winds as modelled here for V5.0.

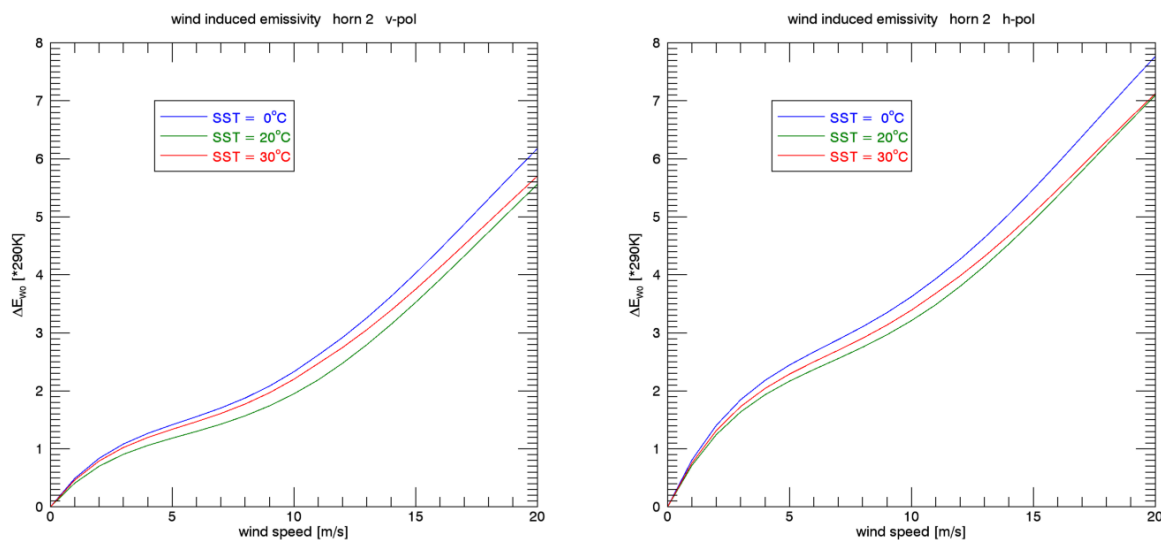


Figure 12: The wind induced emissivity ΔE_{w0} for horn 2 that is used in V5.0 as function of wind speed for 3 different SST values. Left: v-pol. Right: h-pol.

Figure 12 compares the wind-speed dependence of ΔE_{w0} in V5.0 for horn 2 at 3 different SST values. All curves show reasonably smooth behavior as function of wind speed w .

This new form for the SST dependence of the wind induced emissivity supersedes the empirical adjustment of the SST dependence that has been used in V4.0 (Addendum IV, section 2.3). There is no additional SST bias adjustment to the retrieved salinity in V5.0, for example, as had been done in V3.0 (Addendum III, section 6).

5.2 Lookup Table for $\Delta E_{w1}(W_{HHH}, \sigma'_{0,vv})$

The lookup table for $\Delta E_{w1}(W_{HHH}, \sigma'_{0,vv})$ has been rederived for V5.0. This resulted in a small change compared with the values from Meissner et al. (2014), which were used in V3.0 and V4.0. The updated values are listed in Table 3 of Appendix B of this Addendum.

5.3 Correction for Significant Wave Height

The correction $\Delta E_w(W_{HHH}, SWH)$ has been eliminated in V5.0. With the model updates, the size of this correction has been found to be very small. This applies if and only if scatterometer observations (W_{HHH} and $\sigma'_{0,vv}$) are used in the surface roughness correction. As it has been shown in Meissner et al. (2014), if using NCEP wind speeds in the roughness correction, then the SWH contribution ΔE_{w2} can be sizeable.

5.4 1st Guess Salinity Field in the HHH Wind Speed Retrieval

The HHH wind speed retrievals need a 1st guess salinity as input (Meissner et al., 2014; ATBD version 2, Section 2). For V5.0, the 1st guess salinity field is a monthly 2° climatology of salinity maps that have been retrieved from Aquarius data using HH wind speeds in the roughness correction and using the update models for the reflected galaxy correction (Section 3 of this Addendum) and O₂ absorption (Section 4 of this Addendum).

6 Sensor Calibration and Drift Correction

6.1 Calculation of TA Expected

For calculating TA expected, Version 5.0 uses the monthly Scripps ARGO field as reference salinity (Section 2 of this Addendum) instead of HYCOM.

6.2 Rain Filter

When performing the wiggle correction (Addendum III, Section 7) in V5.0, the Aquarius data are filtered for rain in addition to the masks and flags that were established in Addendum III (Addendum III, Sections 7.3 and 7.4) to define data to be used for calibration. In particular, Aquarius observations are not used when calculating the running 7-day global average of $TA_{\text{measured}} - TA_{\text{expected}}$, if the instantaneous rain rate IRR (Appendix C of this Addendum) exceeds 0.25 mm/h. The rain filter is being applied to avoid mismatch between Aquarius and ARGO salinity due to possible salinity gradients in the upper ocean layer created by precipitation (Boutin et al., 2016). Aquarius measures surface salinity within the upper few centimeters of the ocean layer and in the case of a stratified upper ocean layer and the presence of precipitation, the Aquarius SSS are fresher than those from ARGO, which measures at 5-meter depth.

6.3 Closure Between Sensor Calibration and Salinity Retrieval

The calibration drift correction is based on matching $TA_{\text{measured}} - TA_{\text{expected}}$ for global 7-day averages (Addendum III, section 7).

There are small inconsistencies between the calculation of the differences between measured and expected TA and the calculation of the differences between measured and expected $TB_{\text{sur},0}$. The $TB_{\text{sur},0}$ is the TB at a flat ocean surface after the surface roughness correction. In the calculation of TA_{expected} the HH wind speed needs to be used because calibrated Aquarius TB are not yet available at that stage of the algorithm. The surface roughness correction in the salinity retrieval algorithm uses HHH wind speeds. The HHH and HH wind speeds do not exactly match and thus sensor calibration and retrieval do not exactly match either. This results in small biases of about 0.003 K - 0.013 K between the measured and expected values of $TB_{\text{sur},0}$. The values of the biases are channel dependent. Other small biases of the same size between the measured and expected values of $TB_{\text{sur},0}$ are caused by the correction for

land intrusion (ATBD Version 2). The correction is applied in the salinity retrieval algorithm when the antenna weighted land fraction exceeds 0.005. In the forward model calculation of TA expected this correction has not been applied.

Table 1: In V5.0 the values in this table are subtracted from $T_{B_{sur,0}}$ measured in order to enforce closure between sensor calibration and salinity retrievals.

Channel	1V	1H	2V	2H	3V	3H
Bias [K]	-0.013	-0.015	-0.021	-0.023	-0.020	-0.018

As a consequence of the small biases between the measured and expected values of $T_{B_{sur,0}}$ there are also small biases in the retrieved Aquarius SSS when compared to ARGO. The SSS bias increases with decreasing SST. In V5.0 closure between calibration and retrieval is enforced by subtracting the observed small biases in $T_{B_{sur,0_measured}} - T_{B_{sur,0_expected}}$ from the measured $T_{B_{sur,0_measured}}$ before the MLE of the salinity retrieval algorithm is performed. The values of these biases are listed in Table 1. They are different for each channel and are constant in time.

7 MLE Weights in the Salinity Retrievals

In V5.0 equal weights are used for computing the χ^2 of the MLE in the salinity retrieval algorithm. That means, that equation (9) of Addendum III, Section 4 now has the form:

$$\chi^2 = \left[T_{B,0,V}^{measured} - T_{B,0,V}^{RTM}(T_S, SSS) \right]^2 + \left[T_{B,0,H}^{measured} - T_{B,0,H}^{RTM}(T_S, SSS) \right]^2 \quad (14)$$

8 References

Boutin, J. et al. (2016), Satellite and In Situ Salinity: Understanding Near-Surface Stratification and Subfootprint Variability. *Bull. Amer. Meteor. Soc.*, 97, 1391–1407, doi: 10.1175/BAMS-D-15-00032.1.

Brucker, L., E. P. Dinnat, and L. S. Koenig (2014), Weekly gridded Aquarius L-band radiometer/scatterometer observations and salinity retrievals over the polar regions-Part 2: Initial product analysis, *Cryosphere*, 8(3), 915–930, doi:10.5194/tc-8-915-2014.

Comiso, J. C. (2009), Enhanced Sea Ice Concentrations and Ice Extents from AMSR-E Data, *Journal of The Remote Sensing Society of Japan*, 29(1), 199–215, doi:10.11440/rssj.29.199.

Dinnat, E. P., D. M. Le Vine, S. Abraham, and N. Floury (2010), Map of Sky Background Brightness Temperature at L-Band [Online]. Available: <http://oceancolor.gsfc.nasa.gov/AQUARIUS/DinnatEtAl2010>.

Dinnat, E. P., and L. Brucker (2016), Improved Sea Ice Fraction Characterization for L-Band Observations by the Aquarius Radiometers, *IEEE Transactions on Geoscience and Remote Sensing*, doi:10.1109/TGRS.2016.2622011.

Joyce, R. J., J. E. Janowiak, P. A. Arkin, and P. Xie (2004), CMORPH: A method that produces global precipitation estimates from passive microwave and infrared data at high spatial and temporal resolution. *J. Hydrometeorol.*, 5, 487-503. doi:10.1175/1525-541(2004)005<0487:CAMTPG >2.0.CO;2.

LeVine, D. M., and S. Abraham (2004), Galactic noise and passive microwave remote sensing from space at L-band, *IEEE Transactions on Geoscience and Remote Sensing*, 42 (1), 119-129.

Liebe, H. J., P. W. Rosenkranz, and G. A. Hufford (1992), Atmospheric 60-GHz oxygen spectrum: New laboratory measurements and line parameters, *J. Quant. Spectrosc. Radiat. Transfer*, 48, 629–643.

Meissner, T., F. Wentz and L. Ricciardulli (2014), The emission and scattering of L-band microwave radiation from rough ocean surfaces and wind speed measurements from the Aquarius sensor, *JGR Oceans*, vol. 119, doi: 10.1002/2014JC009837.

Meissner, T., F. Wentz, J. Scott, and J. Vasquez-Cuervo (2016), Sensitivity of Ocean Surface Salinity Measurements from Spaceborne L-Band Radiometers to Ancillary Sea Surface Temperature, *IEEE TGRS*, vol. 54(12), pp 7105 - 7111, doi:10.1109/TGRS.2016.2596100.

Misra, S. and S. T. Brown, (2017), Enabling the Extraction of Climate-Scale Temporal Salinity Variations from Aquarius: An Instrument Based Long-Term Radiometer Drift Correction, in *IEEE TGRS*, vol. 55 (5), pp. 2913-2923.

Santos-Garcia, A., H. Ebrahimi, Y. Hejazin, M. M. Jacob, W. L. Jones, and W. Asher (2014a), Application of the AQ rain accumulation product for investigation of rain effects on AQ Sea Surface Salinity measurements. *Microwave Radiometry and Remote Sensing of the Environment (MicroRad)*, 2014 13th Specialist Meeting on, (pp. 72-77). Pasadena, CA. doi:10.1109/MicroRad.2014.6878911.

Santos-Garcia, A., M. M. Jacob, W. L. Jones, W. Asher, Y. Hejazin, H. Ebrahimi, and M. Rabolli (2014b), Investigation of rain effects on Aquarius Sea Surface Salinity measurements. *J. Geophys. Res: Oceans*, 119, 7605-7624. doi:10.1002/2014JC010137.

Santos-Garcia, A., M. M. Jacob, and W. L. Jones (2016), SMOS Near-Surface Salinity Stratification Under Rainy Conditions. *IEEE Journal of Selected Topics in Applied Earth Observations and Remote Sensing*, 1-7. doi:10.1109/JSTARS.2016.2527038.

Soldo, Y, P. De Matthaëis, and D.M. Le Vine (2016), L-band RFI in Japan, Proc. 2016 Radio Frequency Interference Conference, Socorro, NM, pp 111-114, October, 2016, DOI: 10.1109/RFINT.2016.7833542.

Wentz, F., and T. Meissner (2016), Atmospheric Absorption Model for Dry Air and Water Vapor at Microwave Frequencies below 100 GHz Derived from Spaceborne Radiometer Observations, Radio Sci., 51, doi:10.1002/2015RS005858.

Appendix A. Tabulated Values for $\rho'(T_s)$

Table 2: Tabulated values for the SST dependence of $\rho'(T_s)$ in (12) for all Aquarius channels. The units are dimensionless.

T_s [°C]	1V	1H	2V	2H	3V	3H
0.5	0.11014	0.05057	0.09397	0.03676	0.06955	0.0189
1.5	0.084	0.03483	0.06403	0.01906	0.04087	0.00894
2.5	0.06925	0.02804	0.04925	0.01471	0.02359	0.00565
3.5	0.04954	0.0173	0.03051	0.0096	0.00599	0.00186
4.5	0.02831	0.00571	0.01243	0.00343	-0.01136	-0.00173
5.5	0.01441	-0.00195	-0.002	-0.0025	-0.02646	-0.00568
6.5	-0.0002	-0.01176	-0.01515	-0.00876	-0.04226	-0.01108
7.5	-0.01114	-0.01873	-0.02571	-0.01444	-0.049	-0.01418
8.5	-0.02068	-0.02492	-0.03898	-0.02056	-0.05944	-0.01741
9.5	-0.03149	-0.03217	-0.04829	-0.02467	-0.06945	-0.02143
10.5	-0.04418	-0.04024	-0.06129	-0.03017	-0.08742	-0.02695
11.5	-0.05339	-0.04559	-0.06639	-0.03292	-0.09151	-0.02982
12.5	-0.05914	-0.0492	-0.07051	-0.03566	-0.09534	-0.03175
13.5	-0.0707	-0.05349	-0.08155	-0.04215	-0.1079	-0.03756
14.5	-0.07465	-0.0555	-0.08462	-0.04307	-0.10706	-0.0378
15.5	-0.074	-0.05335	-0.08079	-0.04298	-0.10488	-0.03808
16.5	-0.07005	-0.04972	-0.07283	-0.04093	-0.0947	-0.03627
17.5	-0.06916	-0.04675	-0.0741	-0.04116	-0.09439	-0.03862
18.5	-0.06043	-0.0405	-0.05889	-0.03528	-0.07884	-0.03309
19.5	-0.05259	-0.03459	-0.04962	-0.03005	-0.06237	-0.02893
20.5	-0.04119	-0.02761	-0.03796	-0.02552	-0.04306	-0.02447
21.5	-0.04039	-0.02543	-0.03344	-0.0215	-0.03189	-0.02209
22.5	-0.01632	-0.00978	-0.00693	-0.01024	0.00267	-0.00931
23.5	-0.00326	0.00085	0.00547	-0.00317	0.02184	-0.00309
24.5	0.00929	0.01154	0.01911	0.00472	0.04186	0.00433
25.5	0.02281	0.0223	0.03957	0.01544	0.06183	0.01339
26.5	0.02853	0.03028	0.04985	0.02299	0.07005	0.02091
27.5	0.03666	0.04371	0.06703	0.03911	0.09149	0.03475
28.5	0.05908	0.06171	0.08902	0.05218	0.1135	0.04452
29.5	0.08866	0.08612	0.12319	0.07194	0.15642	0.06523

Appendix B. Tabulated Values for $\Delta E_{w1}(W, \sigma'_{0,vv})$

Table 3: Tabulated values of $\Delta E_{w1}(W, \sigma'_{0,vv})$ for the 3 Aquarius horns. The 1st column is wind speed W . The second column is $\sigma'_{0,vv}$, whose intervals are different for each horn. The 3rd column is the number of observation that went into the bin. The 4th column is the value of ΔE_{w1} for v-pol (times 290 K). The 5th and last column is the value of ΔE_{w1} for h-pol (times 290 K). If the values of W or $\sigma'_{0,vv}$ fall outside the values listed in the table, then the value of ΔE_{w1} is set to the lowest or highest end listed in the table, respectively.

radiometer 1				
0.5	0.0040	23500	0.02057	0.13311
0.5	0.0120	39818	-0.00413	0.09059
0.5	0.0200	42541	-0.03463	0.01295
0.5	0.0280	13659	-0.07929	-0.17207
0.5	0.0360	1194	-0.15937	-0.37159
1.5	0.0200	11022	0.06206	0.26406
1.5	0.0280	55462	-0.01998	0.08312
1.5	0.0360	83413	-0.04778	-0.00523
1.5	0.0440	54583	-0.08109	-0.13359
1.5	0.0520	8726	-0.12577	-0.32589
2.5	0.0360	4630	0.07305	0.28361
2.5	0.0440	62365	-0.03426	0.07122
2.5	0.0520	147590	-0.06309	-0.04681
2.5	0.0600	95490	-0.07819	-0.16249
2.5	0.0680	3942	-0.12069	-0.32316
3.5	0.0520	10595	-0.00079	0.15636
3.5	0.0600	195777	-0.04066	-0.00472
3.5	0.0680	301339	-0.04484	-0.08681
3.5	0.0760	16234	-0.07761	-0.17216
4.5	0.0600	4643	0.02995	0.19948
4.5	0.0680	351581	-0.01743	0.02680
4.5	0.0760	470637	-0.03456	-0.05618
4.5	0.0840	32332	-0.07245	-0.16211
5.5	0.0680	18416	0.03255	0.17114
5.5	0.0760	744483	-0.01434	0.01884
5.5	0.0840	400839	-0.04142	-0.08513
5.5	0.0920	32320	-0.08378	-0.19611
6.5	0.0760	117301	0.03634	0.12157
6.5	0.0840	1145819	-0.00932	-0.00879
6.5	0.0920	226601	-0.05696	-0.14283
6.5	0.1000	9135	-0.10590	-0.25063
7.5	0.0760	2489	0.25252	0.41515
7.5	0.0840	563356	0.03493	0.07007
7.5	0.0920	1021366	-0.00758	-0.04363
7.5	0.1000	56939	-0.11230	-0.22043
8.5	0.0840	47274	0.15661	0.26609
8.5	0.0920	1069217	0.02920	0.03178
8.5	0.1000	355659	-0.02299	-0.09609
8.5	0.1080	5851	-0.27842	-0.38250
9.5	0.0840	3191	0.23774	0.40303
9.5	0.0920	239005	0.07635	0.15111
9.5	0.1000	843773	0.02540	0.00262
9.5	0.1080	74727	-0.05366	-0.17136

9.5	0.1160	3506	-0.36642	-0.44547
10.5	0.0920	24455	0.13057	0.26825
10.5	0.1000	414517	0.04278	0.09587
10.5	0.1080	423506	0.02432	-0.03220
10.5	0.1160	19872	-0.09904	-0.23465
10.5	0.1240	2240	-0.36465	-0.43538
10.5	0.1320	651	-0.43946	-0.49745
11.5	0.0920	1733	0.16102	0.36485
11.5	0.1000	68855	0.06006	0.19112
11.5	0.1080	394026	0.02012	0.05644
11.5	0.1160	208526	0.01797	-0.06771
11.5	0.1240	9144	-0.08709	-0.24983
11.5	0.1320	1406	-0.28047	-0.37517
12.5	0.1000	6270	0.08314	0.28717
12.5	0.1080	99342	0.01408	0.13836
12.5	0.1160	300473	-0.00038	0.02477
12.5	0.1240	122159	-0.00369	-0.10259
12.5	0.1320	7343	-0.05462	-0.25285
12.5	0.1400	908	-0.13846	-0.32683
13.5	0.1080	9909	0.03245	0.24969
13.5	0.1160	94398	-0.01348	0.11371
13.5	0.1240	213287	-0.02859	-0.00387
13.5	0.1320	87981	-0.03990	-0.13603
13.5	0.1400	7827	-0.06663	-0.27719
13.5	0.1480	1074	-0.05255	-0.31871
14.5	0.1080	766	0.18480	0.48222
14.5	0.1160	10737	0.01241	0.23460
14.5	0.1240	72161	-0.03579	0.09903
14.5	0.1320	145958	-0.05975	-0.02715
14.5	0.1400	66695	-0.07679	-0.16237
14.5	0.1480	8369	-0.09813	-0.29489
14.5	0.1560	1300	-0.06509	-0.34599
15.5	0.1160	782	0.12291	0.44741
15.5	0.1240	8557	0.00090	0.23763
15.5	0.1320	48834	-0.05503	0.08837
15.5	0.1400	96256	-0.08946	-0.04489
15.5	0.1480	52475	-0.11586	-0.18382
15.5	0.1560	9236	-0.13473	-0.31199
15.5	0.1640	1515	-0.12293	-0.37679
16.5	0.1240	746	0.10370	0.42214
16.5	0.1320	6282	0.00206	0.24243
16.5	0.1400	30642	-0.06995	0.08578
16.5	0.1480	59813	-0.11531	-0.05359
16.5	0.1560	39468	-0.14964	-0.19583
16.5	0.1640	9040	-0.16797	-0.31653
16.5	0.1720	1593	-0.18317	-0.41135
17.5	0.1320	634	0.17014	0.48265
17.5	0.1400	4159	0.01530	0.26649
17.5	0.1480	18459	-0.06964	0.09665
17.5	0.1560	36767	-0.13390	-0.05927
17.5	0.1640	27599	-0.18167	-0.20972
17.5	0.1720	7827	-0.21152	-0.33943
17.5	0.1800	1702	-0.19374	-0.40574
18.5	0.1480	2724	0.05799	0.29760
18.5	0.1560	11001	-0.05055	0.11188
18.5	0.1640	21445	-0.13113	-0.05141
18.5	0.1720	18568	-0.20429	-0.21262
18.5	0.1800	6926	-0.23978	-0.34191
18.5	0.1880	1758	-0.21817	-0.41082
19.5	0.1560	1702	0.09345	0.33100

19.5	0.1640	6394	-0.02639	0.14393
19.5	0.1720	11431	-0.10909	-0.02614
19.5	0.1800	11242	-0.18780	-0.19093
19.5	0.1880	5366	-0.23084	-0.32255
19.5	0.1960	1553	-0.22976	-0.40767
20.5	0.1640	1253	0.06979	0.31419
20.5	0.1720	3636	0.00102	0.15977
20.5	0.1800	6198	-0.08366	-0.00855
20.5	0.1880	6667	-0.16218	-0.16955
20.5	0.1960	3823	-0.23393	-0.31010
20.5	0.2040	1226	-0.26223	-0.41752
21.5	0.1720	1032	0.13268	0.33712
21.5	0.1800	2234	0.02520	0.16010
21.5	0.1880	3459	-0.06938	-0.00061
21.5	0.1960	3711	-0.13306	-0.13637
21.5	0.2040	2501	-0.21806	-0.28504
22.5	0.1800	844	0.11734	0.29603
22.5	0.1880	1326	0.01029	0.12908
22.5	0.1960	1921	-0.04284	0.00219
22.5	0.2040	1885	-0.10316	-0.11506
23.5	0.1880	508	0.08219	0.25175
23.5	0.1960	923	0.02653	0.11305
23.5	0.2040	1204	-0.01815	0.00692
24.5	0.1960	537	0.04951	0.19922
24.5	0.2040	729	0.02267	0.10655

radiometer 2

0.5	0.0015	9357	-0.03047	0.07216
0.5	0.0045	21187	-0.02674	0.07159
0.5	0.0075	31792	-0.03837	0.05096
0.5	0.0105	31531	-0.06323	-0.02424
0.5	0.0135	9710	-0.10843	-0.21319
0.5	0.0165	951	-0.18632	-0.40445
1.5	0.0105	12682	0.02341	0.22158
1.5	0.0135	49163	-0.02820	0.07952
1.5	0.0165	71981	-0.05179	-0.00060
1.5	0.0195	50149	-0.07857	-0.12066
1.5	0.0225	12419	-0.10824	-0.29095
1.5	0.0255	819	-0.15298	-0.42559
2.5	0.0165	6348	0.05531	0.26438
2.5	0.0195	59331	-0.02752	0.08959
2.5	0.0225	132069	-0.04835	-0.03627
2.5	0.0255	88422	-0.05757	-0.16193
2.5	0.0285	7722	-0.09712	-0.29606
3.5	0.0195	771	0.15218	0.36033
3.5	0.0225	35507	0.00250	0.14128
3.5	0.0255	242128	-0.01506	-0.00521
3.5	0.0285	179850	-0.03356	-0.11709
3.5	0.0315	9377	-0.13090	-0.23650
4.5	0.0225	1296	0.12412	0.31707
4.5	0.0255	144146	0.01802	0.10676
4.5	0.0285	514297	-0.00392	-0.01778
4.5	0.0315	92028	-0.07366	-0.14495
4.5	0.0345	10568	-0.16538	-0.26571
5.5	0.0255	43406	0.06311	0.19106
5.5	0.0285	700134	0.00345	0.03466
5.5	0.0315	296107	-0.04211	-0.08626
5.5	0.0345	50362	-0.12083	-0.21746
5.5	0.0375	5976	-0.19537	-0.32013
6.5	0.0255	5545	0.11711	0.27172

6.5	0.0285	534419	0.02271	0.06763
6.5	0.0315	704534	-0.02648	-0.04771
6.5	0.0345	97593	-0.09753	-0.19440
6.5	0.0375	20563	-0.17497	-0.29428
6.5	0.0405	746	-0.24428	-0.37667
7.5	0.0285	208529	0.04574	0.11177
7.5	0.0315	1052029	-0.00658	-0.01909
7.5	0.0345	175833	-0.06894	-0.14818
7.5	0.0375	25512	-0.16236	-0.25016
8.5	0.0285	32584	0.07405	0.18586
8.5	0.0315	771020	0.02344	0.03808
8.5	0.0345	480282	-0.02596	-0.08121
8.5	0.0375	17217	-0.17207	-0.20075
9.5	0.0285	977	0.08206	0.24037
9.5	0.0315	234700	0.05196	0.12420
9.5	0.0345	690325	0.01289	-0.00795
9.5	0.0375	100986	-0.01622	-0.12152
9.5	0.0405	1466	-0.30970	-0.28618
10.5	0.0315	20517	0.06525	0.21338
10.5	0.0345	340047	0.04071	0.09001
10.5	0.0375	380827	0.01515	-0.03477
10.5	0.0405	32195	0.01161	-0.15534
10.5	0.0435	891	-0.25057	-0.26598
11.5	0.0315	1080	0.11636	0.34365
11.5	0.0345	46349	0.05492	0.19177
11.5	0.0375	286329	0.02965	0.07337
11.5	0.0405	222190	0.02096	-0.04335
11.5	0.0435	22493	0.02569	-0.16266
11.5	0.0465	865	-0.12292	-0.25389
12.5	0.0345	2700	0.14091	0.36077
12.5	0.0375	51643	0.05042	0.19524
12.5	0.0405	207278	0.01849	0.06991
12.5	0.0435	159382	0.01051	-0.04386
12.5	0.0465	25496	0.01395	-0.16231
12.5	0.0495	1538	-0.04442	-0.26606
13.5	0.0375	3082	0.12849	0.36587
13.5	0.0405	37682	0.04360	0.20760
13.5	0.0435	136588	0.00440	0.07611
13.5	0.0465	128497	-0.01028	-0.03536
13.5	0.0495	34532	-0.00840	-0.15254
13.5	0.0525	3583	-0.02285	-0.25724
13.5	0.0555	564	-0.05328	-0.30838
14.5	0.0405	2643	0.13540	0.37826
14.5	0.0435	22193	0.04536	0.23308
14.5	0.0465	82110	-0.00848	0.08854
14.5	0.0495	98526	-0.02679	-0.01753
14.5	0.0525	40459	-0.03133	-0.12891
14.5	0.0555	6456	-0.02624	-0.22608
14.5	0.0585	806	-0.06792	-0.32454
15.5	0.0435	1808	0.15189	0.41779
15.5	0.0465	12801	0.04986	0.26100
15.5	0.0495	44222	-0.01304	0.11136
15.5	0.0525	68681	-0.04621	-0.00423
15.5	0.0555	42142	-0.06422	-0.11574
15.5	0.0585	10529	-0.06182	-0.21292
15.5	0.0615	1515	-0.05901	-0.29132
16.5	0.0465	1069	0.19774	0.47916
16.5	0.0495	6041	0.09201	0.31493
16.5	0.0525	22534	0.00199	0.15094
16.5	0.0555	42625	-0.04678	0.02082

16.5	0.0585	34878	-0.08015	-0.09671
16.5	0.0615	13841	-0.09393	-0.20362
16.5	0.0645	2978	-0.09816	-0.29274
16.5	0.0675	515	-0.13162	-0.38255
17.5	0.0495	532	0.21508	0.49634
17.5	0.0525	3067	0.11632	0.35521
17.5	0.0555	10906	0.02259	0.19110
17.5	0.0585	22972	-0.03535	0.05425
17.5	0.0615	24755	-0.07550	-0.06491
17.5	0.0645	14485	-0.10687	-0.18543
17.5	0.0675	4773	-0.11712	-0.27365
17.5	0.0705	999	-0.10144	-0.34637
18.5	0.0555	1476	0.18261	0.41786
18.5	0.0585	5394	0.06564	0.23619
18.5	0.0615	11768	-0.00957	0.09982
18.5	0.0645	14146	-0.04148	-0.01064
18.5	0.0675	11004	-0.07648	-0.13046
18.5	0.0705	5379	-0.09703	-0.23420
18.5	0.0735	1719	-0.10118	-0.30312
19.5	0.0585	799	0.19357	0.42843
19.5	0.0615	2576	0.09851	0.28675
19.5	0.0645	6064	0.01619	0.14524
19.5	0.0675	7364	-0.00580	0.04527
19.5	0.0705	5917	-0.03672	-0.07367
19.5	0.0735	3940	-0.07743	-0.19145
19.5	0.0765	1571	-0.12577	-0.30342
20.5	0.0615	539	0.19383	0.44122
20.5	0.0645	1763	0.11525	0.30322
20.5	0.0675	3485	0.03512	0.17647
20.5	0.0705	4103	0.01595	0.07174
20.5	0.0735	3814	-0.01836	-0.05111
20.5	0.0765	2615	-0.09246	-0.19142
21.5	0.0675	1026	0.12544	0.31770
21.5	0.0705	2023	0.04059	0.17743
21.5	0.0735	2311	0.01344	0.07666
21.5	0.0765	1774	0.01160	-0.01215
22.5	0.0705	764	0.09365	0.27707
22.5	0.0735	1400	0.03901	0.16929
22.5	0.0765	1199	0.02007	0.07828
23.5	0.0735	696	0.06326	0.23069
23.5	0.0765	796	0.07517	0.16369
24.5	0.0765	517	0.07570	0.21416

radiometer 3

0.5	0.0010	6739	-0.02543	0.10327
0.5	0.0030	19128	-0.03483	0.08980
0.5	0.0050	31394	-0.04829	0.05303
0.5	0.0070	29870	-0.07025	-0.03204
0.5	0.0090	8254	-0.12308	-0.22388
0.5	0.0110	802	-0.21047	-0.39234
1.5	0.0050	1126	0.12417	0.36612
1.5	0.0070	20765	0.00804	0.19306
1.5	0.0090	66808	-0.03070	0.07682
1.5	0.0110	79132	-0.05857	-0.03006
1.5	0.0130	37163	-0.08062	-0.18599
1.5	0.0150	6474	-0.12743	-0.34239
2.5	0.0090	1611	0.10064	0.34588
2.5	0.0110	35850	-0.00180	0.17345
2.5	0.0130	130733	-0.03338	0.01759
2.5	0.0150	126118	-0.04805	-0.12945

2.5	0.0170	14259	-0.08928	-0.26330
3.5	0.0110	996	0.11777	0.34939
3.5	0.0130	41962	0.01086	0.16840
3.5	0.0150	259596	-0.00937	-0.00341
3.5	0.0170	158833	-0.04297	-0.14162
3.5	0.0190	6820	-0.20718	-0.29061
4.5	0.0130	6404	0.07096	0.26086
4.5	0.0150	261756	0.01545	0.07059
4.5	0.0170	390045	-0.01534	-0.06882
4.5	0.0190	42925	-0.15381	-0.23897
4.5	0.0210	3814	-0.26975	-0.37701
5.5	0.0130	1023	0.11943	0.28867
5.5	0.0150	254092	0.02950	0.09875
5.5	0.0170	648874	-0.01041	-0.03165
5.5	0.0190	92959	-0.11785	-0.20524
5.5	0.0210	15785	-0.22344	-0.34106
6.5	0.0150	191033	0.03467	0.10824
6.5	0.0170	926779	-0.00402	-0.00896
6.5	0.0190	166461	-0.08401	-0.16295
6.5	0.0210	21589	-0.18859	-0.28427
7.5	0.0150	84550	0.03563	0.12951
7.5	0.0170	994442	0.01144	0.02167
7.5	0.0190	292942	-0.05179	-0.10092
7.5	0.0210	10210	-0.18298	-0.19878
8.5	0.0150	12538	0.02598	0.17004
8.5	0.0170	646631	0.03579	0.06673
8.5	0.0190	573301	-0.02210	-0.05034
8.5	0.0210	9250	-0.14169	-0.14505
9.5	0.0150	956	0.02500	0.18605
9.5	0.0170	164812	0.04425	0.12516
9.5	0.0190	694735	0.01754	0.01594
9.5	0.0210	129311	-0.02571	-0.10638
9.5	0.0230	947	-0.23325	-0.12132
10.5	0.0170	11911	0.04523	0.19401
10.5	0.0190	288296	0.04599	0.09775
10.5	0.0210	400720	0.01282	-0.01413
10.5	0.0230	40104	-0.00566	-0.13755
10.5	0.0250	807	-0.20330	-0.16316
11.5	0.0170	983	0.05606	0.22970
11.5	0.0190	27322	0.06042	0.18896
11.5	0.0210	254588	0.03787	0.08276
11.5	0.0230	236678	0.01613	-0.02751
11.5	0.0250	30643	0.01413	-0.14891
11.5	0.0270	1221	-0.09724	-0.22074
12.5	0.0190	1806	0.09144	0.26642
12.5	0.0210	31891	0.05781	0.19073
12.5	0.0230	177807	0.02263	0.07726
12.5	0.0250	169967	0.01123	-0.02438
12.5	0.0270	35439	0.01375	-0.13735
12.5	0.0290	2156	-0.02349	-0.21604
13.5	0.0210	2165	0.11305	0.30158
13.5	0.0230	22969	0.06137	0.21627
13.5	0.0250	111515	0.01789	0.08991
13.5	0.0270	134097	-0.00447	-0.01709
13.5	0.0290	43645	-0.01643	-0.12750
13.5	0.0310	4306	-0.02474	-0.21391
13.5	0.0330	549	-0.09206	-0.28491
14.5	0.0230	1658	0.10649	0.29688
14.5	0.0250	12566	0.07260	0.24206
14.5	0.0270	60508	0.01634	0.10974

14.5	0.0290	97540	-0.02045	-0.00233
14.5	0.0310	49703	-0.04023	-0.10906
14.5	0.0330	9674	-0.04184	-0.19837
14.5	0.0350	1247	-0.08100	-0.27999
15.5	0.0250	988	0.11808	0.31307
15.5	0.0270	7018	0.08768	0.26901
15.5	0.0290	31305	0.01696	0.13761
15.5	0.0310	63146	-0.02827	0.01899
15.5	0.0330	46583	-0.05977	-0.08879
15.5	0.0350	15430	-0.06874	-0.18265
15.5	0.0370	2543	-0.05903	-0.23405
16.5	0.0270	585	0.12832	0.36372
16.5	0.0290	3506	0.10354	0.30973
16.5	0.0310	15068	0.03421	0.17556
16.5	0.0330	34531	-0.02914	0.04427
16.5	0.0350	35551	-0.07838	-0.06901
16.5	0.0370	17051	-0.10338	-0.17473
16.5	0.0390	3530	-0.08012	-0.22327
16.5	0.0410	687	-0.06454	-0.26143
17.5	0.0310	1764	0.15023	0.35672
17.5	0.0330	6971	0.08368	0.23563
17.5	0.0350	18560	-0.00976	0.08501
17.5	0.0370	23347	-0.07637	-0.03948
17.5	0.0390	16146	-0.12087	-0.16132
17.5	0.0410	5277	-0.12035	-0.23613
17.5	0.0430	1031	-0.09694	-0.27634
18.5	0.0330	669	0.22257	0.41460
18.5	0.0350	3372	0.12763	0.29064
18.5	0.0370	9135	0.02665	0.13651
18.5	0.0390	12617	-0.04621	0.01865
18.5	0.0410	11291	-0.10863	-0.11629
18.5	0.0430	5592	-0.14798	-0.23497
18.5	0.0450	1378	-0.13022	-0.28591
19.5	0.0370	1835	0.15485	0.31848
19.5	0.0390	4495	0.03731	0.16462
19.5	0.0410	6878	-0.01078	0.05246
19.5	0.0430	6681	-0.09623	-0.08185
19.5	0.0450	4350	-0.16377	-0.22455
19.5	0.0470	1578	-0.21793	-0.34842
20.5	0.0390	1080	0.11120	0.27654
20.5	0.0410	2641	0.06148	0.17252
20.5	0.0430	3897	0.01093	0.07500
20.5	0.0450	3568	-0.04318	-0.03801
20.5	0.0470	2584	-0.12595	-0.18413
20.5	0.0490	1218	-0.20497	-0.32823
21.5	0.0410	952	0.13938	0.28301
21.5	0.0430	1936	0.06653	0.17349
21.5	0.0450	2153	0.01518	0.08291
21.5	0.0470	1973	-0.03825	-0.03550
21.5	0.0490	1401	-0.14055	-0.21466
21.5	0.0510	630	-0.31801	-0.41702
22.5	0.0430	752	0.14147	0.26010
22.5	0.0450	1087	0.06885	0.16872
22.5	0.0470	1150	0.05218	0.09049
22.5	0.0490	1053	-0.04162	-0.04944
22.5	0.0510	829	-0.21291	-0.30128
23.5	0.0450	567	0.16008	0.26491
23.5	0.0470	735	0.06295	0.14223
23.5	0.0490	715	-0.00125	0.05170
23.5	0.0510	748	-0.15284	-0.16842

Appendix C. Rain Accumulation Product

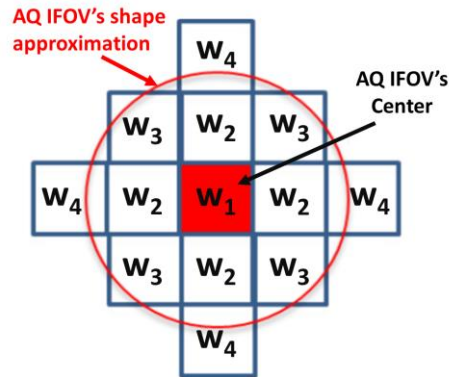


Figure 13: Spatial model used to calculate average instantaneous rain rate and rain accumulation over an Aquarius IFOV. Boxes are 0.25° lat/lon grid cells.

The Aquarius Rain Accumulation (RA) product (Santos-Garcia et al., 2014a, 2014b, 2016) is to provide an ancillary data set that aids users of Aquarius Level 2 data to better understand the salinity stratification changes due to rain. This product provides the rain history over the previous 24 hours to the Aquarius measurement time and provides a quantitative estimate of the surface salinity stratification. This Aquarius RA product was an initiative that made possible the development of the Rain Impact Model (RIM) that was initially applied to Aquarius and further extended to other data sets as SMOS (Santos-Garcia et al., 2014b, 2016). This RA data product is an overlay of the Aquarius L2 science data product (SSS retrieval) that contains relative probability of salinity stratification (PS), rain beam fraction (BF), instantaneous rain rate (IRR) averaged over the IFOV (Individual Field of View) and rain accumulation (RA). The product uses as input the surface rain rates from the NOAA CMORPH (CPC-Climate Prediction Center-Morphing technique) global precipitation data set (Joyce et al., 2004). The average instantaneous rain rate is calculated using a structure of 13 CMORPH pixels around the center of the Aquarius IFOV as is shown in Figure 13, where the weight associated with each pixel is based on the antenna radiometric main beam efficiency. More detailed information

about the dataset are found in the document “Readme file for the CFRSL – Rain Impact Model (RIM) v1.2 for Aquarius” associated with the RIM data set. A subset of essential RIM parameters is included in the Aquarius L2 product, e.g. IRR, PSS, BF, rain impacted ancillary salinity (HYCOM) and rain caused salinity change at surface (0.05 meters in depth), 1, 3 and 5 meters below surface.

Appendix D. Ancillary Sea Ice Fraction

The ancillary product and the computation for the sea ice fractions have been updated to better match changes in the Aquarius TB induced by sea ice entering the field of view (FOV). A summary of the changes is provided here. More details can be found in Dinnat and Brucker (2016).

Sea ice has a much larger TB than sea water. Therefore, only a small fraction of sea ice in the FOV is needed to significantly increase TB. In order to filter out TB contaminated by sea ice, a sea ice fraction (SIF) is reported for each Aquarius observations in the level 2 products. The SIF is derived by integrating a map of sea ice concentrations (SIC) over the beam FOV after weighting by the antenna gain pattern. There are various ancillary products available for SIC. In algorithm version V4.0 (and before), Aquarius used the SIC from NOAA Marine Modeling and Analysis Branch (MMAB). Figure 14 reports a comparison of the SIC from NOAA MMAB with another SIC product derived from AMSR2 observation and the bootstrap algorithm (Comiso, 2009). There are some very substantial differences in both the products in the marginal zone and inside the ice pack. Brucker et al. (2014) identified significant discrepancies between TB measured by Aquarius and SIF reported in previous versions of the product. The Aquarius TB in V4 does not correlate very well with the SIF computed from NOAA MMAB SIC, exhibiting a highly non-linear behavior and very large scatter (Figure 15, red). The new

model for SIF (Figure 15, blue) computed from AMSR2 SIC show a much-improved relationship between TB and SIF, with strong linear relationship and much reduced scatter. Because of sensor availability during Aquarius period of observations, here are the ancillary sources used as function of time (all using bootstrap algorithm):

- AMSRE-Bootstrap: 08-25-2011 – 10/04/2011
- SSMIS-Bootstrap: 10/05/2011 – 07/02/2012 & [05/10/2013 – 05/14/2013]*
- AMSR2-Bootstrap: 07/03/2012 – 06/07/2015 (excl. *)

The data sources are:

- AMSR-E: ftp://n5eil01u.ecs.nsidc.org/SAN/AMSA/AE_SI12.003/
- SSMIS: ftp://sidacs.colorado.edu/pub/DATASETS/nsidc0079_gsfc_bootstrap_seaice/
- AMSR2: gcom-w1.jaxa.jp

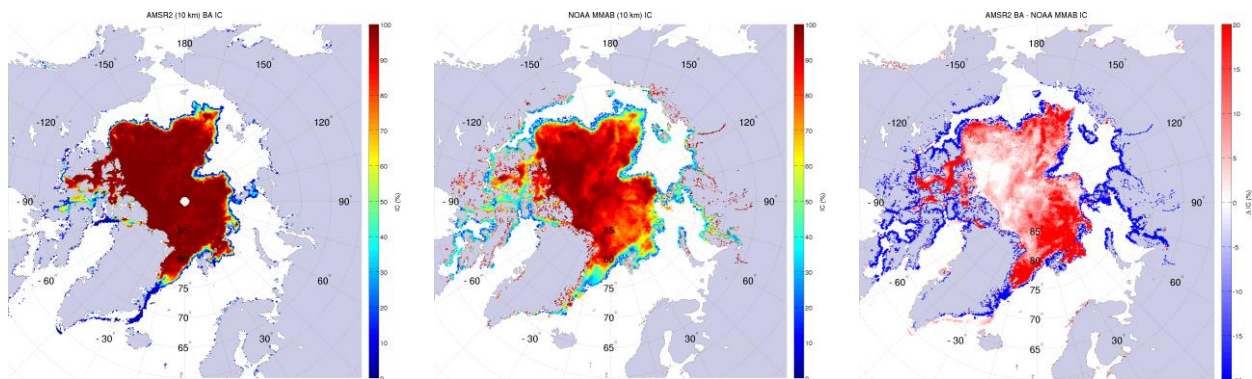


Figure 14: Sea ice concentration map on October 1, 2014 in the Northern hemisphere from (left) the AMSR2 bootstrap product and (middle) the NOAA MMAB product. (Right) difference in sea ice concentration maps between AMSR2 and NOAA MMAB.

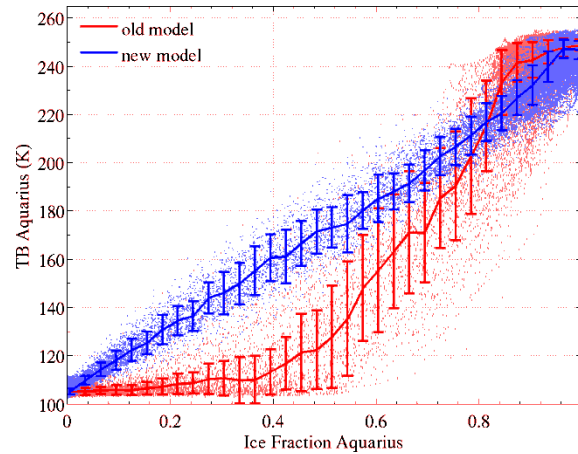


Figure 15: Aquarius observed brightness temperature (TB) as a function of ice fraction in the instruments field of view (V-pol, beam 1) in the Ross Sea near Antarctica. The red data use the old ice fraction model (using NOAA MMAB ice concentrations) as reported in the Aquarius product (V4.0). The new model (in blue) uses boot-strap-based ice concentration products and exhibits a much better match between ice fraction and changes in observed TB.

Appendix E. Instrument-Only Calibration Drift Correction for Residual Pseudo-Periodic Oscillations (“Wiggles”)

As explained in ATBD Addendum II Section IV and Addendum III Section 7 and Appendix E, the Aquarius instrument exhibits a time dependent drift which manifests itself in a bias in $TA_{\text{measured}} - TA_{\text{expected}}$. A correction for the pseudo-periodic oscillations in this drift, called “wiggles” (Addendum III Appendix E2), has been developed that uses a hardware based correction that only requires inputs from the Aquarius radiometer and does not depend on an external reference salinity field. The oscillations are termed “pseudo” because the calibration anomaly is not periodic in nature and only has the appearance of periodicity. The instrument-only correction for the pseudo-periodic oscillations as part of the instrument calibration is explained in this appendix.

The blue dots in Figure 16 shows the “wiggle” part of the calibration drift in TA as function of orbit number for all six Aquarius channels.

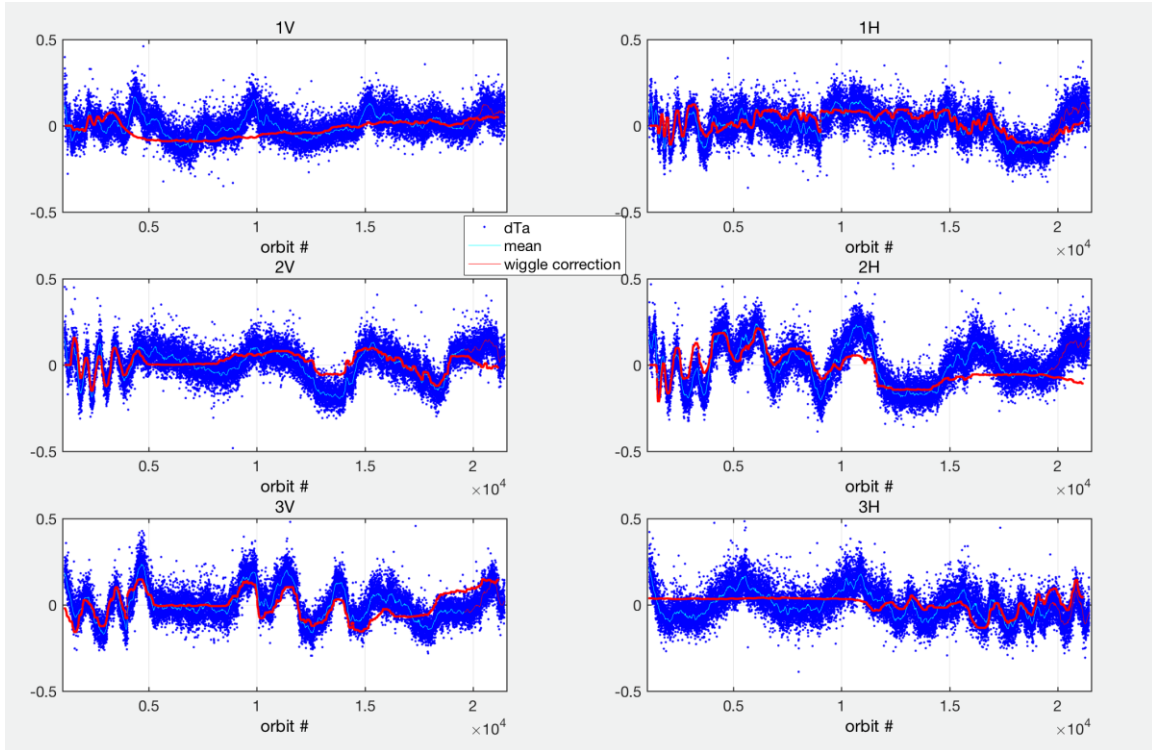


Figure 16: Blue dots: Wiggle part of $TA_{\text{measured}} - TA_{\text{expected}}$ for all Aquarius orbits. Blue line: its mean value. Red line: Derived instrument-only wiggle correction.

The root cause for this part of the calibration drift was determined to be a locking issue in the backend Voltage to Frequency Converter (VFC), which impacts all counts of the radiometer including the reference load (Long Accumulation, or LA) counts (Figure 17). VFC locking is a phenomenon that occurs when the output locks on to a certain frequency even though the input voltage to the VFC is changing. As the radiometer gain drifted over time as the amplifiers aged, the reference counts varied over a wide range going through many locking frequencies. This had the effect of trapping the LA counts at a particular value for some period of time. Figure 18 shows a histogram of uncalibrated antenna counts for all six channels from 550 to 660 over a one and half-year period of the mission. The curves would typically be smooth, with a large number of histogram values when observing the ocean over a smaller dynamic

range and a relatively lesser number of values when observing land over a larger dynamic range. The spikes represent locking values due to the VFC, which are the same for all six channels regardless of their relative calibration.

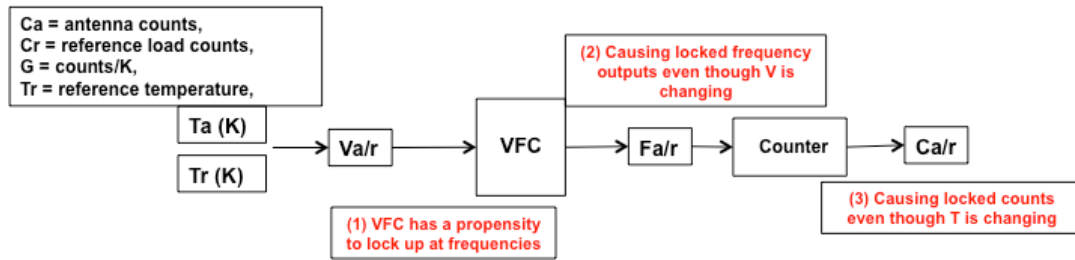


Figure 17: Flow diagram showing how the frequency lock affects the reference count readings.

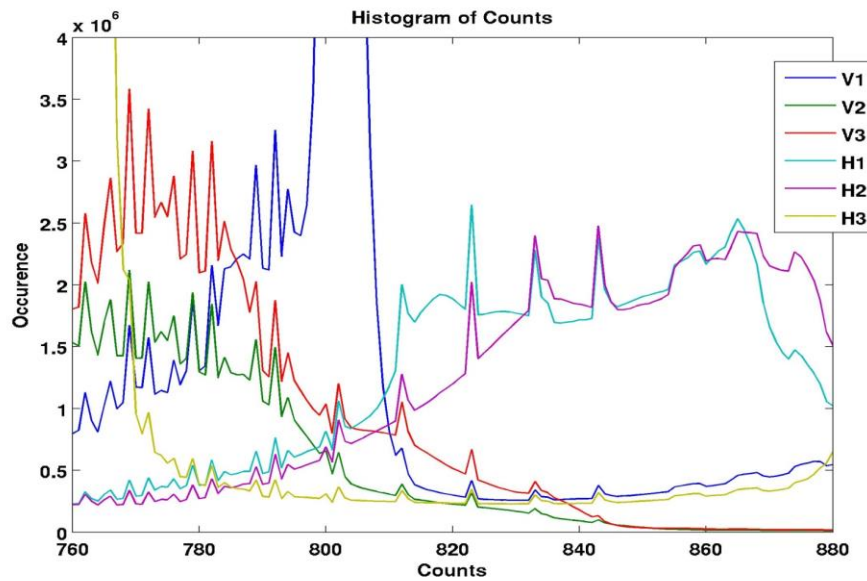


Figure 18: Histogram of frequency locked long accumulation counts for both V and H channels of all 3 beams.

In order to fix this locking problem, a correction to the affected reference counts has been derived using the difference between consecutive samples of the reference load count. Consecutive reference load samples were observed to have a constant bias between them, resulting in the reference load counts getting locked at different times. The cause for this bias is likely due to offsets in the backend that vary with radiometer switching state. A delta value is calculated by numerically solving a differential equation of the reference load differences. The solution produces the magnitude of added wiggle as a function of absolute reference load value.

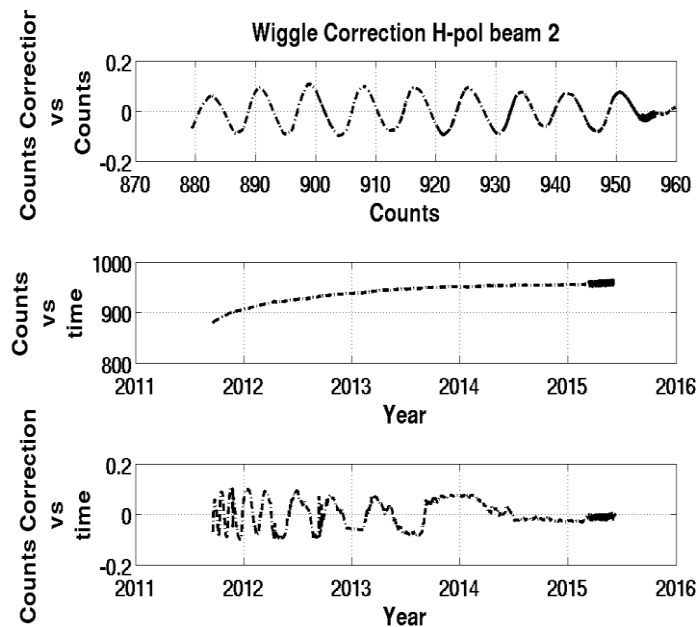


Figure 19: An example of corrections for channel 2H for the frequency lock effect.

This correction is done before nonlinearity correction to raw counts. To implement the pseudo-periodic oscillation correction in the radiometer calibration, the delta value is subtracted from the normalized long accumulation counts (LA). This delta is found by locating a closest count value in a look up table (different for each of the 6 channels, 1V, 1H, 2V, 2H, 3V and 3H) and reading the corresponding adjustment. This process is illustrated in Figure 20. The derived LA correction is shown by the red curves in Figure 16. Detailed description of the correction can be found in Misra and Brown (2017).

Appendix F. Land Emission Model

Changes have been made to model used for emissivity over land in the Aquarius forward algorithm (TA_expected). The new model:

- Addresses some issues with the previous land model.
- Improves consistency with the land model used in the SMAP soil moisture retrieval algorithm.

The following modifications have been made to address issues with the existing model:

- Extrapolation of available the ancillary soil moisture to fill some missing values near the coasts.
- Use of the weighted fractions of land and sea ice outside of the ocean calibration regions.
- Use of look up tables to compute the emissivity of frozen regions (the look up tables have been created by computing the emissivity from the Aquarius measurements and averaging over the entire duration of the mission).
- Estimation of the fraction of frozen land from the Land Surface Temperature distributed by GEOS v5.

- Compute the Faraday rotation angle from theory using the IGS TEC (only over land).

The following changes have been made to improve the consistency of the model with the model used by SMAP. This was done mainly by adding or changing the sources of ancillary datasets. In particular:

- Land classification: use land classification from MODIS IGBP.
- Vegetation opacity: compute vegetation opacity from the NDVI obtained from MODIS climatology.
- Roughness parameter: source now land-cover dependent roughness parameters, as provided in the SMAP L2 Soil Moisture (Passive) ATBD, v4.0, Table 3.
- Single-scattering albedo coefficient: source now land-cover dependent roughness parameters, as provided in the SMAP L2 Soil Moisture (Passive) ATBD, v4.0, Table 3. This required new equations for the reflectivity of the surface after the vegetation layer. The new equations are reported below.
- Clay/sand map: use same maps as SMAP. They are obtained by merging some regional databases (STATSGO, NSDC, ASRIS) with the HWSD (Harmonized World Soil Database);
- Dielectric mixing model: use the Mironov model instead of the Dobson model.
- Land surface temperature: use temperatures from GEOS-5.
- Soil moisture: use soil moisture from GEOS-5.

The vegetation and roughness corrections now use the following equation:

$$\begin{aligned}
 R_{rough,P} &= R_{smooth,P} \cdot e^{-h} \\
 R_{obs,P} &= 1 - (1 - \omega) \cdot (1 - \gamma) \cdot \left(1 + R_{rough,P} \gamma\right) - \left(1 - R_{rough,P}\right) \gamma
 \end{aligned}
 \tag{15}$$

where:

- R = reflectivity
- $smooth$ = Reflectivity of the smooth surface (obtained from Fresnel's equations)
- $rough$ = Reflectivity at the surface, i.e. after roughness correction but before the vegetation
- obs = Predicted observed reflectivity
- P = polarization (H or V)
- h = roughness parameter
- ω = single-scattering albedo
- $\gamma = e^{-\tau sec(\theta)}$
- τ = one-way transmissivity of the vegetation canopy

The land model before and after the updates has been compared against the measurements over 1 week (1st week of 2014). The correlation coefficients and the RMSE for the different channels are reported in Table 4 below. The new land model is slightly better for all channels.

Table 4: Correlation coefficients and RMSEs, for all the Aquarius channels, comparing the measured antenna temperatures and the antenna temperatures estimated using the land model before and after the updates.

	Correlation coefficient		RMSE [K]	
	before update	after update	before update	after update
beam1-V	0.987	0.991	11.97	11.16
beam2-V	0.989	0.994	10.59	9.41
beam3-V	0.989	0.995	9.80	7.50
beam1-H	0.985	0.989	13.74	13.21
beam2-H	0.985	0.990	13.80	12.82
beam3-H	0.984	0.989	14.40	12.98

Appendix G. RFI Filtering

The Aquarius RFI detection algorithm relies on detecting outliers among the 10-ms samples. Although many RFI signals are correctly detected with this approach, certain RFI signals (e.g. a random collection of many small, independent emitters) looks similar to natural noise. These sources can be strong (Soldo et al., 2016) and the transition from natural to RFI-dominated regions may be slow and resemble the transition between sea and land scenes. For these reasons such sources of RFI are often missed with the existing Aquarius detection algorithm.

A threshold criterion has been added to the RFI detection algorithm for V5.0 to aid in resolving this problem. The threshold is applied the mean TA at 1.44 s (the fundamental Aquarius data block).

The thresholds are set to be the highest antenna temperatures we expect from the natural scene. They are calculated using the forward model (TA_expected) using the updated land emissivity model and assuming:

- Soil moisture = 0 (perfectly dry soil).
- Surface temperature = 340 K.
- No attenuation from the vegetation layer or the atmosphere.

The thresholds for V5.0 for each of the channels are listed in Table 5.

Table 5: TA threshold values used in V5.0.

	V-polarization	H-polarization
Beam1	339 K	327 K
Beam2	344 K	321 K
Beam3	350 K	315 K

Antenna temperatures higher than these thresholds are flagged as RFI. As additional precaution, the antenna temperatures within 10 s of a flagged sample are also flagged as RFI (see Figure 20).

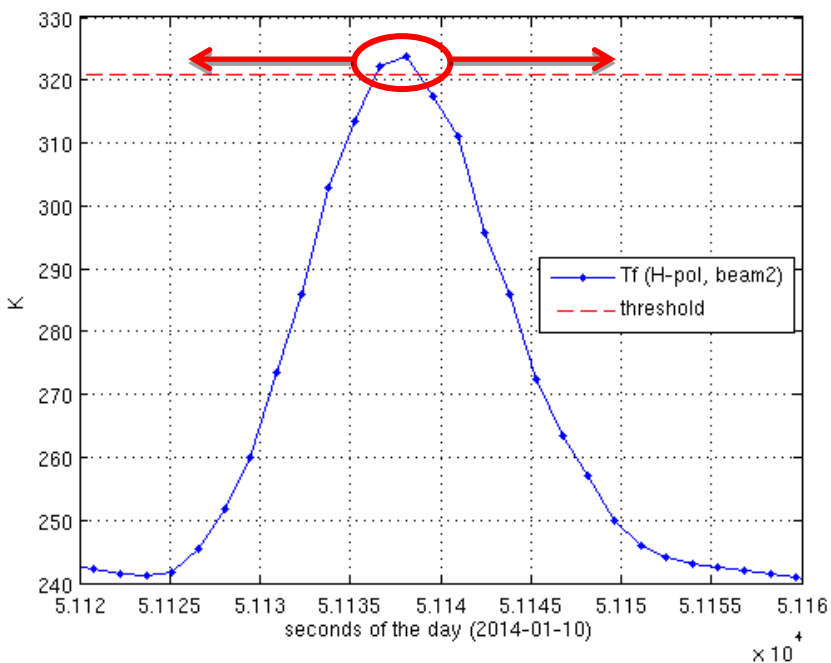


Figure 20: Time series of the antenna temperature after RFI filtering over an RFI source in Russia using the RFI algorithm without the threshold. Two samples are higher than the threshold (red dashed line). The red arrows indicate the samples that will be flagged as RFI with the new criteria (samples that exceeded the threshold plus neighbors within 10s).

Appendix H. Full-Range Calibration

The goal of Aquarius is to map sea surface salinity, and the calibration is focused on this goal. However, there are other potential applications of the measurements (e.g. soil moisture) and to accommodate such uses a second calibration has been developed so that the data cover the

full range from cold sky to ocean and land. The changes are small and have minimal effect on the data over ocean, but to be sure to not impact the retrieval of SSS, this calibration is being offered as research product (V5.1) separate from V5.0.

The objective of the Whole Range Calibration (WRC) is to adjust the radiometer calibration in order to match radiometric observations to simulations of antenna temperatures (“expected” TA) over the full range of TA. To do this, observations and simulations over the celestial sky (~ 5 K) are used in addition to those over the ocean (~ 100 K) to determine a linear correction for the radiometer. Using the large dynamic range helps determine the slope as a function of the target TA in a way not possible with only ocean observations which have a small dynamic range.

The WRC will not impact significantly the SSS retrievals, because the observations over the ocean are already empirically calibrated (for their global average) using the simulations. As for the adjustment in gain introduced by the WRC, it is largely mitigated by: 1) the small dynamic range of TA over the ocean and 2) the empirical adjustments operated on the SSS retrieval algorithm (e.g. the roughness impact on TB surface). The impact of the WRC will be seen mostly for observation of the celestial sky (for which biases exist in V5) and warm TA over land and ice. The objective of the WRC is not to improve SSS retrieval but to improve the retrieved TB of the surface at the warm and cold ends to allow for science applications other than SSS and inter-comparisons with over L-band sensors over the sky or land/ice.

The adjustment to TA is made according to the expression:

$$T_{A,new} = a \cdot T_{A,old} + b \quad (16)$$

with $T_{A,new}$ the updated Aquarius observation using the WRC and $T_{A,old}$ the Aquarius Ta before WRC as found in V5.0. The coefficient a corrects gain inaccuracies and b corrects for a constant bias. The coefficients are derived from linear regression between two points:

- At the cold end, with $T_{A,old}$ the median of the TA measured by Aquarius for the 30 cold sky calibrations and $T_{A,new}$ the median of the simulated TA for the cold sky calibration.
- Over the ocean, with $T_{A,old}$ the median of the TA measured by Aquarius globally for the year 2012 (with RFI filtered, water fraction of $\geq 99.9\%$) and $T_{A,new}$ the median of the corresponding simulations (“TA expected”).

Table 6 reports the results for the computation of the coefficients a and b :

Table 6: Values for the coefficients a and b .

	V-pol		H-pol	
	a	b	a	b
Beam 1	1.0029392655	-0.3206818726	1.0065873947	-0.6021517766
Beam 2	1.0078767991	-0.9153618782	1.0028942038	-0.2617863425
Beam 3	1.0170156871	-2.1531981034	1.0006834163	-0.0730229557